Yaroshenko, V., Lühr, H. (2016): Electrical conductivity of the dusty plasma in the Enceladus plume. - *Icarus*, *278*, pp. 79–87.

DOI: http://doi.org/10.1016/j.icarus.2016.05.033

Electrical conductivity of the dusty plasma in the Enceladus plume

V.V. Yaroshenko[a,*], H. Lühr[a]

[a] *GFZ German Research Center For Geosciences, Telegrafenberg, 14473 Potsdam, Germany*

Abstract

The plasma conductivity is an important issue for understanding the magnetic field structure registered by Cassini in the Enceladus proximity. We have revise the conductivity mechanism to incorporate the plume nanograins as a new plasma species and take into account the relevant collisional processes including those accounting for the momentum exchange between the charged dust and co-rotating ions. It is concluded that in the Enceladus plume the dust dynamics affects the Pedersen and Hall conductivity more efficiently than the electron depletion associated with the presence of the negatively charged dust as has been suggested by (*Simon et al.*, 2011). The electron depletion remains a decisive factor for only the parallel conductivity. In the parameter regime relevant for the Enceladus plume, one finds increase of the Pedersen and decrease of the parallel components, whereas for the Hall conductivity the charged dust changes both - its value and the sign. The associated reversed Hall effect depends significantly upon the local dust-to-plasma density ratio. An onset of the reversed Hall effect appears to be restricted to outer parts of the Enceladus plume. The results obtained can significantly modify Enceladus' Alfvén wing structure and thus be useful for interpretations of the magnetic field perturbations registered by the Cassini Magnetometer during the close Enceladus flybys.

Keywords: `Saturn, satellites; Enceladus, Saturn, magnetosphere;`

*V. V. Yaroshenko

Email addresses: `yarosh@gfz/potsdam.de` (V.V. Yaroshenko), `hluehr@gfz/potsdam.de` (H. Lühr)

1. Introduction

The Enceladus' plume discovered recently by the Cassini orbiter (*Porco et al.*, 2006) creates a remarkable space object consisting of a mixture of neutral gas and dust grains with the usual plasma constituents. Indeed, the multiple water vapor jets emanating from the south pole region of the small moon (radius $R_E \simeq 252$ km) are contaminated with numerous icy particles whose sizes are ranged from nano- to micrometer scales. The dust grains ejected into the magnetospheric plasmas and radiative environment become electrically charged by various processes, the most effective one being capture of electrons and ions from the co-rotating plasma flows. The latter provides mainly negative particle charges and the consequent electron depletion (*Yaroshenko et al.*, 2014). Although to date there is no general consensus between the Cassini Plasma Spectrometer (CAPS) observations of charged nanograins and plasma imbalance measured by the Cassini Langmuir probe (see e.g. discussions in (*Hill et al.*, 2012; *Dong et al.*, 2015; *Yaroshenko et al.* , 2015)), here we address the CAPS measurements of charged nanograins. During a few plume encounters the Cassini Plasma Spectrometer detected a dust population with mass-to-charge ratios $m_d/q_d \sim 10^4$ amu/e and cumulative dust number density up to $n_d \sim 10^3$ cm^{-3} (*Hill et al.*, 2012). Such charged nano-particles, bridging the mass gap between the macromolecules and larger solid icy grains, together with usual microparticles (electrons, ions and neutrals) generate a specific plasma region which extends more than ~ 1000 km in space and is associated with the name "plume". Physically, this region represents a low-temperature weakly ionized dusty plasma (*Yaroshenko and Lühr*, 2015).

Once a dust grain is charged, it starts to react to electromagnetic forces in addition to the ordinary gravitational ones. Hence there is a coupling to the ambient plasma through electromagnetic fields, regardless whether these are pre-existent or self-induced. This has opened up many new problems such as charged dust transport (*Horány et al*, 2004; *Hsu et al*, 2004; *Dong et al.*, 2015; *Meier et al.*, 2014; *Farrell et al.* , 2014), dust contribution to the plasma shield-

ing (*Yaroshenko and Lühr*, 2015) and modifications of the plasma conductivity mechanism with a possible feedback of the charged grains to the magnetic field perturbations measured by the Cassini magnetometer (MAG) at the moon's proximity (*Simon et al.*, 2011; *Kriegel et al.*, 2011, 2014).

The main goal of our present theoretical study is to investigate the plasma conductivity of a dusty plasma. The idea of the dust influence on the plasma conductivity has been put forward by *Simon et al.* (2011). They built up a model of the Alfvén wing system that is generated by the interaction between the Enceladus plume and the co-rotating plasma in Saturn's inner magnetosphere. Using the theoretical findings by *Neubauer* (1980;1998), and *Saur et al.* (1999;2007), *Simon et al.* (2011) showed that the observed orientation of the magnetic field may arise due to the presence of immobile negatively charged dust grains in the plume, serving as a sink for "free" magnetospheric electrons and providing the negative sign of the Hall conductivity (the reversed Hall effect). As a consequence, the component of the magnetic field perturbations towards and away from Saturn is also reversed in accordance with measurements of the Cassini magnetometer during the plume encounters. One of the conclusions of this study however is that the considered submicron-sized grains mainly contribute to the Enceladus/plasma interaction by absorbing the ambient electrons while the contribution of dust transport to the magnetic field perturbations can safely be neglected. Since then several numerical studies have been carried out to interpret the magnetic field and plasma observations during the available Cassini encounters with the plume (see (*Kriegel et al.*, 2011, 2014) and references herein). The numerical approach by Kriegel et al. 2014 has included tiny, nano-sized grains in the modeling of the perturbed magnetic field. These studies however also supported the conclusion that the magnetic field distortions in the plume region are mainly associated with an accumulation of negative charge density on the grains and the consequent electron depletion.

At the same time, as has been discussed in a very recent paper (*Yaroshenko and Lühr*, 2015), the numerous negatively charged nanograins with charge-to-mass ratios detected by the CAPS instrument ($m_d/q_d \sim 10^4$ amu/e) are mainly gov-

erned by the Lorentz force while the gravitational forces remain weaker already at distances $R \sim$100 km $< R_E$ from the moon's surface. Furthermore, the estimates of the plasma parameter defined as the number of grains in the Debye sphere $N = 4\pi\lambda_{Dd}^3 n_d/3$ (here λ_{Dd} and n_d are the dust Debye length and dust density, respectively) are typically in the range $N \sim 10^5 - 10^6$. These variations are illustrated as color-coded plots along the Cassini plume trajectories for E3 and E5 flybys in Fig.1. Therefore, the plasma approximation seems to be fully appropriate for the tiny nanograins as now the dust is an essential ingredient of the total plasma mixture. Hence collective effects associated with the charged grains become important. The paper by (*Yaroshenko and Lühr*, 2015) addresses a simplified model of the plasma conductivity due to the incorporation of the dust grains as additional heavy ions. In this study, we include dust charging and grain dynamics in a self-consistent way to advance the plasma conductivity tensor formalism. Moreover, our present approach additionally invokes the exchange momentum between the plasma and dust particles (i.e. the plasma drag force) which can be relevant in the Enceladus plume due to the relative plasma-dust drift.

2. Basic formalism

2.1. Plume model

The plume of Enceladus is the multispecies medium. The main constituents include neutral gas (water vapor), magnetospheric electrons and various positive ions (mainly of the water group), as well as charged dust. The dust grains come in all sizes ranging from nanometer scales to large solid icy particles. The combination of the impact data by the Cassini Dust Analyzer (CDA) and the Radio and Plasma Wave Instrument (RPWS) with CAPS data obtained during available plume encounters indicate that a size distribution can be described by a power law $dn_d \propto a^{-4} da$, (where a being the particle size) (*Dong et al.*, 2015). For such steeply decaying distribution the cumulative dust number density and charge density will be mainly determined by smallest nano-sized grains, viz.

$n_d = \int_{a_{min}}^{a_{max}} dn_d \propto a_{min}^{-3}$ and $\sigma_d \propto \int_{a_{min}}^{a_{max}} a dn_d \propto a_{min}^{-2}$, when $a_{min} \ll a_{max}$. Moreover, it is tacitly assumed that the smallest particles can reach their equilibrium charges during the residence time in the plume (*Yaroshenko and Lühr* , 2014). Then to first approximation, the problem of the dust size distribution can be reduced to the case of monodisperse dust, introducing a single grain species with $a = a_{min}$, i.e. of nanometer-scales whose mass-to-charge ratio is close to $m_d/q_d \sim 10^4$ amu/e and density varies in the range $n_d \sim 0.1{-}10^3$ cm^{-3} in accordance with the CAPS measurements inside the plume.

Our analysis will be mainly based on the average estimates listed in Table 1 as discussed by (*Yaroshenko and Lühr*, 2015). The plume parameter regime corresponds to the low-temperature (electron and ion temperatures are around $T_e \sim T_i \sim 1$ eV) weakly ionized plasma with a degree of ionization in the range $\sim 10^{-5} - 10^{-3}$ as follows from the measurements of the Cassini Ion and Neutral Mass Spectrometer (INMS) and the RPWS instrument during the plume flybys (*Morooka et al.*, 2011; *Waite et al.*, 2006). The co-rotating plasma flow withing the dense plume is significantly slowed down (*Tokar et al.*, 2006; *Khurana et al.*, 2007) and an assumption on the subthermal plasma drift (in the moon's frame of reference) seems to be quite reasonable. Note that the measurements of the plasma density in the moon's plume by different Cassini instruments seem to be not consistent (see Fig. 4 in Ref. (*Kriegel et al.*, 2014)) and hence it is reasonable to use a ratio of the dust-to-ion density, n_d/n_i, as a free variable.

2.2. Governing equations

To avoid all ambiguities, we model the plume environment as a four-component magnetized plasma, consisting of thermal electrons (e), positive water group ions (i) , negatively charged dust nano-particles of a single sort (d) and neutrals (n_n) - water molecules. We start from the plasma quasineutrality condition, which now incorporates the dust charge density through

$$n_e + Z_d n_d = n_i, \tag{1}$$

Table 1: Plasma and dust parameters in the Enceladus plume

Parameter	Symbol	Value
Plasma number density	n_0	10^2–10^3 cm^{-3}
Dust number density	n_d	1–10^3 cm^{-3}
Neutral gas density	n_n	10^5–10^9 cm^{-3}
Electron temperature	T_e	$\sim 1-2$ eV
Ion temperature	T_i	$\sim 1-3$ eV
Neural gas/dust gas temperature	$T_n \sim T_d$	200 K
Dust mass-to-charge ratio	m_d/q_d	$\sim 10^4$ amu/e
Ion flow velocity	$\mathbf{u}_0$	< 20 km/s
Local magnetic field	$\mathbf{B}_0$	(0,0,−325) nT
Electron gyrofrequency	ω_{B_e}	5.5×10^4 s^{-1}
Ion gyrofrequency	ω_{B_i}	1.7 s^{-1}
Dust gyrofrequency	ω_{B_d}	3×10^{-3} s^{-1}
Minimal electron-neutral collision mean free path	l_e	10 km
Minimal ion-neutral collision mean free path	l_i	1 km

with n_α being the respective electron, ion and dust ($\alpha = e, i, d$) number density and Z_d denoting the dust charge number. Nano-grains typically carry only a few electrons in equilibrium and in general a stochastic charging model has to be employed to derive Z_d. However the randomly fluctuating charges can also be considered within the standard orbital-motion-limited (OML) formalism *Yaroshenko and Lühr* (2014). It results in stochastic fluctuating grain charges $(0, 1, ...)e$ in the dense dust limit. Fully numerical modeling of the discreet dust charge fluctuations qualitatively leads to similar results (e.g. Fig 2 by *Meier et al.* (2015)). We therefore apply the conventional OML theory (see e.g. (*Horány*, 1996)) for the description of the grain charging inside the moon's plume for reasons of mathematical tractability. Withing this formalism, one can determine the charge number Z_d from the balance of electron and ion currents flowing to and from the grain surface. Written with the help of the charge neutrality (1) this equation is

$$(1 - Z_d n_d/n_i) V_{Te} exp(-Z_d e/(aT_e)) = V_{Ti}(1 + Z_d e/(aT_i)), \tag{2}$$

where $v_{Te(i)} = \sqrt{T_{e(i)}/m_{e(i)}}$ refers to the electron (ion) thermal velocity.

Since we do not distinguish between the plasma electrons, ions and dust particles we treat all of them in the conventional fluid approximation. Following the standard procedure we use the stationary form ($d/dt = 0$) of the momentum equations, in which there are no contributions from the pressure gradient terms and external gravitational forces. For plasma electrons (e), ions (i) and dust (d) these read as

$$\nu_{en}\mathbf{v}_e = -\frac{q_e}{m_e}(\mathbf{E}_0 + \frac{1}{c}[\mathbf{v}_e \times \mathbf{B}_0]), \tag{3}$$

$$\nu_{in}\mathbf{v}_i + \nu_{id}(\mathbf{v}_i - \mathbf{v}_d) = \frac{q_i}{m_i}(\mathbf{E}_0 + \frac{1}{c}[\mathbf{v}_i \times \mathbf{B}_0]), \tag{4}$$

$$\nu_{dn}\mathbf{v}_d + \nu_{di}(\mathbf{v}_d - \mathbf{v}_i) = -\frac{q_d}{m_d}(\mathbf{E}_0 + \frac{1}{c}[\mathbf{v}_d \times \mathbf{B}_0]). \tag{5}$$

Here $\mathbf{v}_\alpha$ is the fluid velocities of the different plasma species having mass m_α and charge q_α ($\alpha = e, i, d$). Furthermore, the particle charges equal $q_e = -q_i = e$ for the plasma electrons and ions, while for the dust grains, $q_d = eZ_d$, where Z_d satisfies the balance of the electron and ion currents as given by Eq. (2). The vectors $\mathbf{E}_0$ and $\mathbf{B}_0$ denote the convective electric field and planetary magnetic field ($\mathbf{E}_0 = -E_0\widehat{\mathbf{y}}$, $\mathbf{B}_0 = -B_0\widehat{\mathbf{z}}$ in the ENIS coordinate system defined in Fig. 1). To illustrate the general effect of the dust dynamics in the plume, we assume the fields $\mathbf{E}_0$ and $\mathbf{B}_0$ to be constant.

The dissipative quantities in Eqs. (3)–(5) $\nu_{\alpha n}$ denote the frequencies of electron-neutral, ion-neutral and dust-neutral collisions, respectively. For the plasma electrons and ions $\nu_{\alpha n}$ are approximated by $\nu_{\alpha n} \simeq n_n \sigma_{\alpha n} v_{T\alpha}$, where n_n is the neutral number density and $\sigma_{\alpha n}$ is the effective collisional cross section. Calculations of the momentum transfer cross section for the electron collisions with water molecules at the electron energy ~ 1 eV lead to $\sigma_{en} \sim 6\times10^{-16}$ cm^2 (see Fig. 7 and Table 5 in Ref. (*Itikawa and Mason*, 2005)). The latter estimate is mainly due to elastic scattering. For the ion effective cross section σ_{in} we use the interpolation given by Cassidy and Johnson, (2010) which accounts for the momentum transfer due to both ion-neutral collisions and charge exchange. At the neutral/ion relative energy ~ 1 eV this yields $\sigma_{in} \sim 3\times10^{-15}$ cm^2.

The momentum transfer frequency in dust-neutral collisions can be described by

the standard Epstein theory (*Epstein*, 1924) leading to $\nu_{dn} = (8\sqrt{2\pi}/3)a^2 n_n m_n v_{Tn}/m_d$, where m_n, n_n and $v_{Tn} = \sqrt{T_n/m_n}$ are the mass, density and thermal velocity of neutrals, respectively. The dust grains, however, introduce some additional peculiarities. In the Enceladus plume there is a relative drift between the dust and plasma components, hence inevitably arises a force related to the momentum transfer from a flowing plasma to charged dust grains and *vice versa*. Including the momentum exchange between the dust and plasma particles (because of $m_i \gg m_e$, only the ion contribution counts) introduces the initial coupling of the ion and dust momentum equations and hence modifying the standard set of equations: the two dissipative terms in Eqs. (4) –(5) $\nu_{id}\,(v_i - v_d)$ and $\nu_{di}\,(v_d - v_i)$ account for the drag of the ions on the dust grains and *vice verse* with ν_{id} being the ion-dust momentum-transfer frequency and the dust-ion momentum-transfer frequency $\nu_{di} = \nu_{id} m_i n_i / m_d n_d$, respectively. Before addressing the conductivity problem, we briefly discuss the relevance of the plasma drag effects for the plume environment.

2.3. Ion drag force

Modeling of the ion drag force has been addressed recently by several authors (a critical examination of the existing theories can be found, e.g., in Refs. (*Fortov et al.*, 2004; *Khrapak and Morfill*, 2009). In all models the force is defined by two effects: the deflection of ions from their original trajectory in the electric field of the charged particle (orbit force) and the collection of ions whose trajectories end on the grain surface (collection force). The general practice in calculation of the collection and orbit force contributions involves the Coulomb radius of ion-grain interactions $r_{\rm C} = Z_d e^2/T_i$. For ions with drift velocity $u_0 \leq v_{Ti}$ and in the collisionless regime, that is a case in the near-Enceladus plasma, the collection force is determined by a cross section $\sigma_c \simeq \left(8\sqrt{2\pi}/3\right) a^2\,(1 + r_{\rm C}/2a)$ (*Fortov et al.*, 2004). A cross section for the orbit force is found from the theory of Coulomb collisions in plasmas based on pure Coulomb interaction potential. When $r_{\rm C}$ is small compared to the plasma screening length, λ_D, this gives a cross section $\sigma_{id} \simeq \left(4\sqrt{2\pi}/3\right) r_{\rm C}^2 \ln\left(T_i \lambda_D / Z_d e^2\right)$ (*Fortov et al.*, 2004). The last factor

in this expression represents a modification of a standard Coulomb logarithm. Assuming that the nanograin charging is adequately described by equation (2), the CAPS limit $m_d/q_d \sim 10^4$ amu/e has been transformed into the dust sizes at given dust fraction (see Fig. 4 in (*Yaroshenko and Lühr*, 2015)). This results in an extremely narrow window of possible grain sizes, a ∼2-3 nm, while the dust-to-plasma density ratio, n_d/n_i, occupies the range (0.1-0.8). Below we always apply these restrictions and keep the mass-charge ratio $m_d/q_d \sim 10^4$ amu/e as a fixed value. Such an approach seems to be adequate for the initial study of plume electrodynamics.

In Fig. 2 we show the ratio of the two cross sections σ_{id}/σ_c as a function of the dust fraction n_d/n_i calculated for various ion temperatures and grain sizes $a \sim 2$ nm and $a \sim 3$ nm. As seen, the ion-dust momentum-transfer cross section at low dust fraction ($n_d/n_i \leq 0.25$) is specified by a value of the Coulomb radius, $r_C > a$. This ensures $\sigma_{id} \gg \sigma_c$ and $\nu_{id} \simeq v_{Ti} n_d \sigma_{id}$ providing a domination of the orbital ion drag force. The latter occurs because of the grains attain comparatively high grain charges $Z_d > 1$ at low n_d/n_i. For the higher dust fractions ($n_d/n_i > 0.3$), the particle charge Z_d is reduced so that mostly $\sigma_{id} \sim \sigma_c$, and the ion-dust collision frequency combines both values of cross sections leading to $\nu_{id} = v_{Ti} n_d (\sigma_{id} + \sigma_c)$. The respective dust-ion collision frequency reads as $\nu_{di} \simeq (\sigma_{id} + \sigma_c) n_i m_i v_{Ti}/m_d$.

In Fig.3 and Fig.4 we show variations in the two collision frequency ratios ν_{id}/ν_{in} and ν_{di}/ν_{dn} with the dust fraction n_d/n_i at various degree of the plasma ionization, assuming $n_i/n_n \leq 10^{-3}$ in accordance with the Cassini data in the plume (*Morooka et al.*, 2011; *Waite et al.*, 2006). As illustrated in Figs. 3-4, both ratios, ν_{id}/ν_{in} and ν_{di}/ν_{dn}, demonstrate maximum values at low dust fraction: ν_{id}/ν_{in} peaks at $n_d/n_i \sim 0.1 - 0.15$, while the dependence for ν_{di}/ν_{dn} reveals a maximum at $n_d/n_i \to 0$. High dust population reduces the equilibrium grain charges Z_d as well as a full cross sections of the ion-dust interactions $(\sigma_{id} + \sigma_c)$ (Fig. 2) and thus decreasing both collisional ratios, ν_{id}/ν_{in} and ν_{di}/ν_{dn} and the role of the plasma-dust interactions. It is also seen that the particle size is an important parameter: as a increases, both frequency ratios also increase, yield-

ing in some cases even a domination of the plasma drag force over the neutral drag force (upper curve at $n_d/n_i \sim 0.1 - 0.2$ in Fig.3). A further remark is that the ion temperature influences significantly both values ν_{in}/ν_{id} and ν_{di}/ν_{dn} . The value of T_i, however, is one of the most uncertain plume parameter. While here the ion temperature is assumed to be close to the electron temperature, it might be lower due to the charge exchange collisions with very cold neutrals ($T_n \sim 0.02$ eV, (*Halevy and Stewart*, 2008)) as has been indicated by (*Tokar et al.*, 2009). Reducing T_i would yield to considerably higher ratios ν_{id}/ν_{in} and ν_{di}/ν_{id} than shown in Figs. 3-4. In any case, Figs. 3-4 indicate that for the realistic plasma conditions and grain sizes the processes associated with momentum transfer from flowing ions to dust grains and *vice versa* might be important for the plume environment and there is the necessity to keep both drag terms in the momentum equations (4)-(5).

3. Conductivity tensor

Continuing the conductivity problem, one solves Eqs. (3)-(5) for the particle speed $\mathbf{v}_\alpha$, (as given in Appendix A), to get the net current density

$$\mathbf{j} = -\sum_\alpha q_\alpha n_\alpha \mathbf{v}_\alpha \tag{6}$$

The Ohm's law represents now a matrix equation $\mathbf{j} = \widehat{\sigma}\mathbf{E_0}$, where the conductivity tensor $\widehat{\sigma}$ is defined by Pedersen (σ_P), Hall (σ_H) and parallel ($\sigma_\parallel$) components as

$$\widehat{\sigma} = \begin{pmatrix} \sigma_P & \sigma_H & 0 \\ -\sigma_H & \sigma_p & 0 \\ 0 & 0 & \sigma_\parallel \end{pmatrix}. \tag{7}$$

The tensor elements are given by

$$\sigma_P = \frac{ec}{B_0}\left(n_e \frac{\eta_e}{1+\eta_e^2} + n_i f_{xx} + n_d Z_d \frac{\eta_d - (\eta_d f_{xy} + f_{xx})\,\frac{\nu_{di}}{\nu_d}}{1+\eta_d^2} \right), \tag{8}$$

$$\sigma_H = \frac{ce}{B_0}\left(n_e \frac{\eta_e^2}{1+\eta_e^2} - n_i f_{xy} + Z_d n_d \frac{\eta_d^2 - (\eta_d f_{xx} - f_{xy})\,\frac{\nu_{di}}{\nu_d}}{1+\eta_d^2} \right), \tag{9}$$

$$\sigma_{\parallel} = e\frac{c}{B_0}\left(n_e\eta_e + n_i f_{zz} + Z_d n_d\left(\eta_d - \frac{\nu_{di}}{\nu_d}f_{zz}\right)\right) \tag{10}$$

Here we denote $\eta_\alpha = \omega_{B\alpha}/\nu_\alpha$, where $\omega_{B\alpha} = |q_\alpha|\, B/cm_\alpha$ is the gyrofrequency of each species and ν_α defines the net momentum-transfer frequencies through $\nu_i = \nu_{in} + \nu_{id}$ for ions and $\nu_d = \nu_{dn} + \nu_{di}$ for dust grains, respectively. For the plasma electrons $\nu_e = \nu_{en}$. The full elements f_{ij} are given in Appendix A.

To simplify the general expressions (8)-(10) and have a manageable discussion when dealing with the plume parameter space, we consider two limiting cases of low and high gas density. The latter varies in the wide range from $\sim 10^5 - 10^6$ cm^{-3} in the outer parts of the plume and up to to $\sim 10^8 - 10^9$ cm^{-3} in the densest central region, as inferred from the measurements of the Cassini Ultraviolet Imaging Spectrograph (UVIS) and from the INMS data during the close Enceladus flybys (*Waite et al.*, 2006; *Hansen et al.*, 2008; *Smith et al.*, 2014; *Dong et al.*, 2011; *Teolis et al.* , 2004). It follows immediately that in both regions for the cross section σ_{en} $\sim 6\times10^{-16}$ cm^2 and $T_e \sim 1-2$ eV the electron-neutral collision frequency will be clearly exceeded by the electron gyrofrequency ($\omega_{Be} \sim 5\times10^5$ s$^-$1) leading to $\eta_e \gg 1$. On the contrary, η_i and η_d admit different relations in two regions: (A) In the parts of the low gas density the condition holds $\eta_e \gg \eta_i > \eta_d > 1$, while the ratio $r = \nu_{id}\nu_{di}/\nu_i\nu_d$, associated with the ion-dust and dust-ion moment exchange, obeys $r \leq 1$; (B) In the high gas density part, $r \ll 1$ and $\eta_d < \eta_i \leq 10$. These two limiting cases, A and B, consistent with the above mentioned periphery of the plume and its dense central region, respectively, will be discussed below.

Case A $\eta_e \gg \eta_i > \eta_d > 1$ and $r \leq 1$

This limit significantly simplifies the expressions for the elements f_{ij} (see Eqs. (A7)-(A9) in Appendix). Inserting the appropriate f_{ij} approximations into Eqs. (8)-(10) and invoking the quasi-neutrality condition (1) leads to the tensor elements

$$\sigma_P \simeq \frac{ec}{B_0}\left(n_i\frac{\nu_{in}}{\nu_i\eta_i} + n_d Z_d\frac{\nu_{dn}}{\nu_d\eta_d}\right), \tag{11}$$

$$\sigma_H \simeq \frac{ce}{B_0}\left(\frac{n_i}{\eta_i^2}\left(1 + \frac{\nu_{id}\nu_{dn}}{\nu_i\nu_d}\frac{\eta_i}{\eta_d}\right) - \frac{Z_d n_d}{\eta_d^2}\frac{\nu_{dn}}{\nu_d}\right), \tag{12}$$

$$\sigma_{\parallel} \simeq \frac{ec}{B_0}\eta_e\left(n_i - Z_d n_d + \frac{\eta_i}{(1-r)\eta_e}(n_i - \frac{\nu_{di}}{\nu_d}Z_d n_d)\right). \quad (13)$$

As is well known all components of the conductivity tensor in the conventional electron-ion plasma are positive. In Figs. 5-7 the solid curves illustrate modifications of the conductivity elements described by Eqs. (11)-(13) with the dust fraction n_d/n_i. In the figures, the tensor components are normalized to their respective value in the conventional plasma, i.e. to σ_{P0}, σ_{H0} or $\sigma_{\parallel 0}$, followed from (8)-(10) at $n_e = n_i$ and $n_d = 0$. It is seen from Fig. 5 that even if the proportion of dust-to ion population is small, its contribution increases the Pedersen term, σ_P, by a factor of a few. At high dust densities, when the negative charge density accumulated by the dust species is of the same order as the ion density, in other words, the Havnes parameter $p = Z_d n_d/n_i \to 1$, the normalized Pedersen component has an upper limit $\sigma_P/\sigma_{P0} \simeq 1 + \eta_{i0}/\eta_{d0}$ determined by the quantities $\eta_{\alpha 0} = \omega_{B\alpha}/\nu_{\alpha n}$, $\alpha = i, d$. This limiting value of σ_P/σ_{P0} can be essentially larger than 1 as shown in Fig. 5. It is interesting enough that the increase of the Pedersen conductivity occurs solely because of the contribution of the dust current. Quite to the contrary, the parallel conductivity in the first order of approximation is mainly determined by the electron depletion due to the presence of the dust species. Indeed, $\sigma_{\parallel} \propto \eta_e(n_i - Z_d n_d)$ and its normalized value $\sigma_P/\sigma_{P0} \propto (1-p)$ decreases with growth of n_d/n_i because of more and more free electrons are accommodated on dust grains. In the extreme limit $p \to 1$, the reduced electron density would lead to negligibly small values of $\sigma_{\parallel}/\sigma_{\parallel 0} \simeq \eta_{i0}/\eta_e \ll 1$ as indicated in Fig. 6. It is important to mention that in the dusty plasma both terms, σ_p and $\sigma_{\parallel}$ necessarily are positive. Contrary to these elements, the Hall conductivity (12) can be either positive or negative depending on the contribution of the charged nanograins (Fig.7). Indeed, the expression (12) introduces a critical value of the Havnes parameter

$$p_{cr} = \frac{\eta_d}{\eta_i}(\frac{\nu_{id}}{\nu_i} + \frac{\eta_d}{\eta_i}\frac{\nu_d}{\nu_{dn}}) \quad (14)$$

so that for $p > p_{cr}$ $\sigma_H < 0$. This condition ensures the reversed direction of the Hall current in the dusty plasma and thus might be of importance for

the interpretations of the magnetic field signatures observed in the vicinity of Enceladus (*Simon et al.*, 2011; *Kriegel et al.*, 2014). The threshold value p_{cr} at the parameter space relevant for the near-Enceladus environment is a weak function of the neutral gas density. Already at the gas density $n_n \geq 10^6$ cm^{-3}, p_{cr} is mainly specified by the second term in Eq. (14), and allows us further to simplify $p_{cr} \simeq \eta_{d0}^2/\eta_{i0}^2$. The latter depends very much on the ion temperature and particle size ($p_{cr} \propto Ta^2$). For the typical nanograin size $a \sim 3$ nm and $T_i \sim 1$ eV it gives $p_{cr} \simeq 5 \times 10^{-2}$. Such values of the Havnes parameter seem to be quite realistic outside the central plume regions. Here the plasma and dust densities are expected to be reduced to $n_i \sim 50 - 100$ cm^{-3} (*Gurnett et al.*, 2004) and to $n_d \sim 1$ cm^{-3} (*Hill et al.*, 2012), respectively. At such a low dust density the grain charge might be enhanced to $Z_d > 1$ and hence provide the necessary value of $p \geq p_{cr}$. This result indicates that an onset of the reversed Hall effect might be associated with outer parts of the plume plasma. Note that the model of (*Simon et al.*, 2011) predicts $p_{cr} \simeq \eta_{i0}^{-2}$ which yields much lower values of $p_{cr} \sim 10^{-6} - 10^{-8}$ for the considered gas density range, $n_n \sim 10^5 - 10^6$ cm^{-3}. These low p_{cr} values do in fact not introduce any obvious threshold for the appearance of the reversed Hall effect. Indeed, the associated with such low p_{cr} dust charge densities ($\sim 10^{-7} - 10^{-9}$) might rather be attributed to the background grain population in the E-ring (*Kempf et al.*, 2008), than to the dust-loaded plume of Enceladus.

Finally coming back to the Hall conductivity (12) a main conclusion is that withing the considered approximation σ_H is primarily governed by the dust dynamics, and already a small fraction of dust particles like $n_d/n_i \geq 10^{-2}$ provides $\sigma_H < 0$, as shown in Fig.7. At the extremely dense dust limit $p \to 1$, the normalized Hall conductivity would be limited by a value $\sigma_H/\sigma_{H0} \simeq (1 + \nu_{id}/\nu_{in})^2 + (\nu_{id}/\nu_{in})(\eta_{i0}/\eta_{d0}) - \eta_{i0}^2/\eta_{d0}^2$. In this expression the last term always dominates ensuring the negative values of σ_H at high dust fractions.

Case B $r \ll 1$ and $\eta_d < \eta_i \leq 10$, while $\eta_e \gg 1$

Under these conditions the elements f_{ij} are given by expressions (A10)-(A12). Substituting these in the tensor elements (8)-(10) and using the plasma quasineu-

trality (1), we retain the most significant terms to get

$$\sigma_P \simeq \frac{ecn_i}{B_0\left(1+\eta_i^2\right)}\left(\eta_i - \frac{\nu_{id}}{\nu_i}\frac{\eta_d\left(1+\eta_d\eta_i\right)}{\left(1+\eta_d^2\right)} + \frac{p}{(1+\eta_d^2)}\left(\eta_d\left(1+\eta_i^2\right) - \frac{\nu_{di}}{\nu_d}\eta_i\left(1+\eta_d\eta_i\right)\right)\right), \tag{15}$$

$$\sigma_H \simeq \frac{ecn_i}{B_0\left(1+\eta_i^2\right)}\left(1 + \frac{\nu_{id}}{\nu_i}\frac{\eta_d\eta_i}{\left(\eta_d^2+1\right)} - \frac{p}{(1+\eta_d^2)}\left(\eta_i^2 + 1 - \frac{\nu_{di}}{\nu_d}\eta_i^2\right)\right), \tag{16}$$

$$\sigma_\parallel \simeq \frac{ecn_i}{B_0}\eta_e\left(1-p\right). \tag{17}$$

To explore the contribution of the dust particles to the conductivity mechanism, we consider the highest values of the dust density $n_n \sim (5-9)\times 10^8$ cm^{-3} measured in the plume center during E5 and E7 flybys by the Cassini INMS (*Dong et al.*, 2011). At such n_n the terms $\propto \nu_{id}/\nu_i$ and ν_{di}/ν_d add only small corrections in the expression between brackets in Eqs. (15)-(16) describing Pedersen and Hall elements. Furthermore the quantity $\eta_\alpha, (\alpha = i, d)$, with a good accuracy, could be replaced by $\eta_{\alpha 0}$. Hence the exchange momentum between the dust and ion plasma species can be safely neglected compared to the retained collisions with neutral molecules. We thus arrive at a simplified expressions for the Pedersen and Hall conductivities as

$$\sigma_P \simeq \frac{ecn_i}{B_0}\left(\frac{\eta_{i0}}{\left(\eta_{i0}^2+1\right)} + p\frac{\eta_{d0}}{(1+\eta_{d0}^2)}\right), \tag{18}$$

$$\sigma_H \simeq \frac{cen_i}{B_0}\left(\frac{1}{\eta_{i0}^2+1} - p\frac{1}{(1+\eta_{d0}^2)}\right). \tag{19}$$

In Figs. 5 and 7 we show additionally to the plots related to the case A the normalized Pedersen and Hall components, described by Eqs. (18) and (19) at the gas density $n_n = 9\times 10^8$ cm^{-3}. As seen the Pedersen and Hall conductivities in case B are considerably lower than those obtained in the case A (compare the appropriate dashed and solid curves in Figs. 5 and 7). On the other hand, both dependencies in dense limit (case B) qualitatively resemble much of the respective curves for σ_P/σ_{P0} and σ_H/σ_{H0}, illustrated the low gas density case

A. Furthermore as we have checked, the parallel component, $\sigma_\parallel/\sigma_{\parallel 0}$ at the considered gas density to a first approximation matches well the corresponding decaying curves of the case A shown in Fig. 6. It is not surprising since both approximations of $\sigma_\parallel$ given by Eq. (17) and Eq. (13) after normalization yield quantities being, to a large extent, specified by the electron depletion, as $\propto (1-p)$.

Finally, the discussion about the dusty plasma conductivity can be rounded of by the looking at the new threshold value of p_{cr} providing the reversed Hall effect in the dense limit:

$$p_{cr} \simeq (1+\eta_{d0}^2)/(1+\eta_{i0}^2) \tag{20}$$

When plotting p_{cr} as a function of the neutral gas density (Fig.8), one obtains typically higher values of p_{cr} than estimates inferred for the plume periphery (e.g. $p_{cr} \sim 5 \times 10^{-2}$ in the case A). Moreover, contrary to the almost constant p_{cr} in the case A, the threshold given by (20) grows as the gas density increases and at the peak gas density $n_n = 9 \times 10^8$ cm^{-3} can reach values up to ~ 0.5. The threshold value increases almost linearly with the ion temperature T_i and squared of the particle size a in a similar way as p_{cr} given by Eq. (14).

We now address the Cassini observations of the plasma and dust densities to ascertain whether the dust density might be really so high to provide $p > p_{cr}$ in the plume center. Introducing a reasonable assumption that the nanograins in the dense part are singly charged ($Z_d = 1$), leads to the lower estimate for the dust population as $n_d/n_i \geq 0.1 - 0.5$. The cumulative dust number density inferred from the CAPS measurements during plume encounters E3 and E5 is about $n_d \sim 10^3$ cm^{-3}. For the plume region one of the main difficulties lies in the proper estimation of the ion density. The interpretations of the Cassini Langmuir probe measurements presented by Morooka et al. (2011) predict a spatially extended region with a strong local enhancement of the ion density up to $n_i \sim 10^4$ cm^{-3} (E3) and even up to $n_i \sim 10^5$ cm^{-3} (E5) in the plume center. Using the along-trajectory profiles of the cumulative dust density (*Hill et al.*, 2012) and ion density (*Morooka et al.*, 2011), one can calculate the vari-

ations of the density ratio n_d/n_i. **In Fig. 8 we indicate the characteristic values $p \sim n_d/n_i \leq 0.1$ (solid diamonds) inferred from the RPWS measurements in the densest part of the plume during the encounter E3 (*Morooka et al.*, 2011).** The simulations by *Kriegel et al.* (2014) based on the magnetic field perturbations lead to a spatially narrower and essentially lower ion density distribution with a maximum $n_i \sim 10^3$ cm^{-3} in the plume center than predictions by *Morooka et al.* (2011). This results in $p \sim n_d/n_i$ values which are almost one order of magnitude bigger (see open diamonds for E3, and open squares for E5 flybys in Fig.8) than the mentioned above estimates of $p \leq 0.1$. Since the Cassini data can ensure such $p \sim n_d/n_i$ that lie above the threshold curves shown in Fig. 8, one can conclude that the dense central part of the plume might change drastically the plasma conductivity and be responsible for the reversed Hall effect. It is worthwhile mentioning here that CAPS detected the peak number density $n_d \sim 10^3$ cm^{-3} during a short time $\delta t \leq 20$ s. Hence one can expect the existence of only a spatially narrow region in the plume, of a scale $\sim \delta t \times V_{SC} \sim 300$ km (the Cassini velocity in the Enceladus frame was $V_{SC} \simeq 14.4$ km/s (E3) and $V_{SC} \simeq 17.7$ km/s (E5)), where the conditions for the negative Hall conductivity might be fulfilled ($p > p_{cr}$).

4. Conclusions

A description has been given of the conductivity tensor in space plasmas containing charged dust with emphasis on the parameter regime relevant for the plasma environment in the vicinity of Saturn's icy moon Enceladus. To deal with the moon's plume, the nanograins were considered as a plasma component, whose charge follow self-consistently variations in the particle density but provides the mass-to charge density close to the CAPS limit. The conductivity formalism hence was advanced to include an unusual heavy charge carrier and to take into account an additional dissipative process associated with momentum exchange between the charged dust and ion plasma species.

Under similar plasma conditions, inclusion of the dust species into the plume

description admits higher values of the Pedersen component and lower values of the parallel conductivity than given by a conventional electron-ion plasma. Moreover, the Hall conductivity achieves significant negative values in the regions of increased dust density. The threshold for the dust charge density providing the reversed Hall effect was worked out for existing domains in the space of compositional parameters. It is concluded that the grain dynamics affects the Pedersen and Hall conductivity more efficiently than the electron depletion associated with the presence of the charged dust as has been suggested by (*Simon et al.*, 2011). The electron depletion remains a decisive factor for the parallel component only. We have illustrated the relevance of our findings in the two specific plume regions - in the low and high gas density domains of the plume. In both regions the difference in the respective tensor elements (with and without dust) can be quite appreciable, and thus a conventional conductivity model can hardly adequate describe electrodynamics of such a dust-loaded plasma environment.

The results obtained can significantly modify Enceladus' Alfvén wing structure (*Simon et al.*, 2011), especially its large-scale properties and thus be useful for understanding the magnetic field perturbations observed by the Cassini orbiter in the Enceladus proximity. **One can expect that the new dust-modified conductivity might also influence the ion pickup process within the plume and its probable coupling with Saturns magnetosphere studied previously by *Pontius and Hill*, (2006).** Furthermore, footprints of the modified electric conductivity might reveal themselves in the magnetic field-aligned electron beams recently sensed by the Cassini RPWS instrument in direct vicinity of the moon as reported by (*Gurnett et al.*, 2011). It has been assumed that the beams map to the transverse magnetic perturbations reported in the magnetometer data and caused by dust-plasma interactions outside of the Enceladus flux tube (*Leisner et al.*, 2013). Finally note, the general analytic results presented here might also be applicable to other space plasmas containing charged dust distributions, for example to charged aerosol clouds in the Earth mesosphere where the physical conditions resemble the cold plasma environment

of the moon's plume.

5. Acknowledgment

This work was supported by the *Deutsche Forschungsgemeinschaft, DFG,* as a part of the Priority Program "Planetary Magnetic Fields", SPP 1488, project number YA 349/1-1.

6. References

Cassidy T. A., and Johnson, R. E., 2010, Collisional spreading of Enceladus neutral cloud Icarus, 209, 696, doi:10.1016/j.icarus.2010.04.010

Dong, Y., T. W. Hill, B. D. Teolis, B. A. Magee, and J. H. Waite 2011, The water vapor plumes of Enceladus,J. Geophys. Res.,116, A10204, doi:10.1029/2011JA016693.

Dong, Y., T. W. Hill, and S.-Y. Ye, 2015, Characteristics of ice grains in the Enceladus plume from Cassini observations, J. Geophys. Res. Space Physics, 120, 915937, doi:10.1002/2014JA020288.

Epstein, P. S., On the Resistance Experienced by Spheres in their Motion through Gases, 1924, Phys. Rev. 23, 710-733, doi.org/10.1103/PhysRev.23.710

W.M. Farrell, J.-E. Wahlund, M. Morooka, D.A. Gurnett, W.S. Kurth, R.J. MacDowall, 2014, An estimate of the dust pickup current at Enceladus, Icarus, 239, 217-221.

Fleshman, B. L., P. A. Delamere, and F. Bagenal, 2010, A sensitivity study of the Enceladus torus, Geophys. Res. Lett, 37, L03202, doi:10.1029/2009GL041613.

Fortov, V E, et al. Dusty plasmas, 2004, Physics Uspekhi, 47 (5) 447 -492, DOI: 10.1070/PU2004v047n05ABEH001689

D. A. Gurnett et al., 2004, The Cassini radio and plasma wave investigation. Space Sci. Rev. 114, 395-463.

D. A. Gurnett et al., 2011, Auroral hiss, electron beams and standing Alfvén wave currents near Saturn's moon Enceladus. Geophys Res. Lett. 38, L06102, doi:10.1029/2011GL046854.

Hansen, C. J.,Esposito, L. W., Stewartet, A. I. F., et al. 2008, Water vapour jets inside the plume of gas leaving Enceladus, Nature, 456, 477-479, doi:10.1038/nature07542

Halevy I and Stewart S T, Is Enceladus plume tidally con- trolled?, 2008, Geophys. Res. Lett.,35, L12203, doi:10.1029/2008GL034349

Hill, T. W., M. F. Thomsen, R. L. Tokar, A. J. Coates, G. R. Lewis, D. T. Young, F. J. Crary, R. A. Baragiola, R. E. Johnson, Y. Dong, R. J. Wilson, G. H. Jones, J.-E. Wahlund, D. G. Mitchell, and M. Horányi, 2012, Charged nanograins in the Enceladus plume, *J. Geophys. Res., 117*, A05209. doi:10.1029/2011JA017218

Horányi, M. 1996, Charged dust dynamics in the Solar system, Annu. Rev. Astrophys., 34, 383-418 DOI: 10.1146/annurev.astro.34.1.383

Horányi, M., T. W. Hartquist, O. Havnes, D. A. Mendis, and G. E. Morfill 2004, Dusty plasma effects in Saturns rings, Rev. Geophys.,42, RG4002, doi:10.1029/2004RG000151

Hsu, H.W., et al., 2011, Cassini dust stream particle measurements during the first three orbits at Saturn 2011, J. Geophys. Res., 116, A08213

Itikawa Y., Mason, N., 2005, Cross Sections for Electron Collisions with Water Molecules, J. Phys. Chem. Ref. Data, 34, 1 http://dx.doi.org/10.1063/1.1799251

Khrapak, S. and Morfill, G. E., 2009, Basic Processes in Complex (Dusty) Plasmas: Charging, Interactions, and Ion Drag Force, Contrib. Plasma Phys. 49, 148-168, DOI: 10.1002/ctpp.200910018

Khurana, K. K., M. K. Dougherty, C. T. Russell, and J. S. Leisner, 2007, Mass loading of Saturns magnetosphere near Enceladus, J. Geophys. Res., 112, A08203, doi:10.1029/2006JA012110

Kempf, S., U. Beckmann, G. Moragas-Klostermeyer, F. Postberg, R. Srama, T. Economou, J. Schmidt, F. Spahn, and E. Grn, 2008, The E ring in the vicinity of Enceladus. Spatial distribution and properties of the ring particles, Icarus, 193, 420437

Kriegel, H., S. Simon, U. Motschmann, J. Saur, F. M. Neubauer, A. M. Persoon, M. K. Dougherty, and D. A. Gurnett, 2011, Influence of negatively charged plume grains on the structure of Enceladus Alfvn wings: Hybrid simulations versus Cassini magnetometer data, J. Geophys. Res., 116, A10223.

Kriegel, H., S. Simon, P. Meier, U. Motschmann, J. Saur, A. Wennmacher, D. F. Strobel, and, M. K. Dougherty, 2014, Ion densities and mag- netic signatures of dust pickup at Enceladus, J. Geophys. Res., 119, 27402774,

Leisner, J. S., Hospodarsky, G. B. and D. A. Gurnett, 2013, Enceladus auroral hiss observations: Implications for electron beam locations, J. Geophys. Res., 118, 160166.

Meier P, Kriegel H., Motschmann U, J. Schmidt, et al., 2014, A model of the spatial and size distribution of Enceladus'dust plume Plan. Space Sci, 104, 216-233.

Meier, P., U. Motschmann, J. Schmidt, et al., 2015, Modeling the total dust production of Enceladus from stochastic charge equilibrium and simulations Plan. Space Sci., 119, 208221.

Morooka, M. W., J.-E. Wahlund, A. I. Eriksson, W. M. Farrell, D. A. Gurnett, W. S. Kurth, A. M. Persoon, M. Shafiq, M. André, and M. K. G. Holmberg (2011), Dusty plasma in the vicinity of Enceladus, J. Geophys. Res., 116, A12221. doi:10.1029/2011JA017038.

Neubauer, F. M., 1980, Nonlinear standing Alfvén wave current system at Io: Theory, J. Geophys. Res., 85, 11711178, doi:10.1029/JA085iA03p01171.

Neubauer, F. M., 1998, The subAlfvénic interaction of the Galilean satellites with the Jovian magnetosphere, J. Geophys. Res., 103, 19,843-19,866, doi:10.1029/97JE03370

Pontius, D. H. and T. W. Hill, 2006, Enceladus: A significant plasma source for Saturns magnetosphere, J. Geophys. Res., 111, A09214, doi:10.1029/2006JA011674

Porco, C. C., et al., 2006, Cassini observes the active south pole of Enceladus, Science, 311, 1393 - 1401

Saur, J., Neubauer,F. M., Strobel,D. F., and Summers, M. E. 1999, Threedimensional plasma simulation of Ios interaction with the Io plasma torus: Asymmetric plasma flow, J. Geophys. Res., 104(A11), 25,10525,126, doi:10.1029/1999JA900304.

Saur, J., F. M. Neubauer, and N. Schilling 2007, Hemisphere coupling in Enceladus asymmetric plasma interaction, J. Geophys. Res., 112, A11209, doi:10.1029/2007JA012479

Simon, S., J. Saur, H. Kriegel, F. M. Neubauer, U. Motschmann, and M. K. Dougherty (2011), Influence of negatively charged plume grains and hemisphere coupling currents on the structure of Enceladus Alfvn wings: Analytical modeling of Cassini magnetometer observations, J. Geophys. Res., 116, A04221, doi:10.1029/2010JA016338.

Smith, H. T., R. E. Johnson, M. E. Perry, D. G. Mitchell, R. L. McNutt, and D. T. Young, 2010, Enceladus plume variability and the neutral gas densities in Saturns magnetosphere, J. Geophys. Res., 115, A10252, doi:10.1029/2009JA015184.

Teolis, B. D., Perry, M. E., Magee, B. A. et al. 2010 *J. Geophys. Res.* **115** Teolis, B. D., M. E. Perry, B. A. Magee, J. Westlake, and J. H. Waite, 2010, Detection

and measurement of ice grains and gas distribution in the Enceladus plume by Cassinis Ion Neutral Mass Spectrometer, J. Geophys. Res., 115, A09222, doi:10.1029/2009JA015192.

Tokar, R. L., R. E., Johnson, T. W. Hill, et al. , 2006, The interaction of the atmosphere of Enceladus with Saturn's Plasma, Science, 311, 1409-1412.

Tokar, R. L., R. E. Johnson, M. F. Thomsen et al. , 2009, Cassini detection of Enceladus cold water-group plume ionosphere, Geophys. Res. Lett. 36, L13203, doi:10.1029/2009GL038923.

Waite, J. H., Jr., et al. (2006), Cassini ion and neutral mass spectrometer: Enceladus plume composition and structure, Science,311, 14191422, doi:10.1126/science.1121290

Yaroshenko, V. V., H. Lühr and W. J. Miloch, 2014, Dust charging in the Enceladus torus, J. Geophys. Res. Space Physics, 119, 221236, doi:10.1002/2013JA019213.

Yaroshenko, V. V. and Lühr H. 2014, Random dust charge fluctuations in the near-Enceladus plasma, J. Geophys. Res., 119, 6190-6198.

Yaroshenko V. V. and Lühr H. 2015, Dusty plasma of the Enceladus plume, Plasma Phys. Contr. Fusion, 58, 014010.

Yaroshenko, V. V., W. J. Miloch and Lühr H. 2015, Particle-in-cell simulation of spacecraft/plasma interactions in the vicinity of Enceladus, Icarus, 257, 18.

Appendix A. Derivation of the conductivity tensor

Solving the set of momentum equations (3)-(5) for the particle velocities $\mathbf{v}_\alpha$ yields

$$v_e = \frac{c}{B_0}\begin{pmatrix} -\frac{\eta_e}{(1+\eta_e^2)} & -\frac{\eta_e^2}{(1+\eta_e^2)} & 0 \\ \frac{\eta_e^2}{(1+\eta_e^2)} & -\frac{\eta_e}{(1+\eta_e^2)} & 0 \\ 0 & 0 & -\eta_e \end{pmatrix}\mathbf{E}_0, \tag{A.1}$$

$$\mathbf{v}_i = \frac{c}{B_0}\begin{pmatrix} f_{xx} & -f_{xy} & 0 \\ f_{xy} & f_{xx} & 0 \\ 0 & 0 & f_{zz} \end{pmatrix}\mathbf{E}_0, \tag{A.2}$$

$$\mathbf{v}_d = \frac{c}{B_0}\begin{pmatrix} \frac{-\eta_d+(\eta_d f_{xy}+f_x)\frac{\nu_{di}}{\nu_d}}{\left(1+\eta_d^2\right)} & -\frac{\eta_d^2-(\eta_d f_x-f_{xy})\frac{\nu_{di}}{\nu_d}}{\left(1+\eta_d^2\right)} & 0 \\ \frac{\eta_d^2-(\eta_d f_x-f_{xy})\frac{\nu_{di}}{\nu_d}}{\left(1+\eta_d^2\right)} & \frac{-\eta_d+(\eta_d f_{xy}+f_x)\frac{\nu_{di}}{\nu_d}}{\left(1+\eta_d^2\right)} & 0 \\ 0 & 0 & \left(-\eta_d+\frac{\nu_{di}}{\nu_d}f_{zz}\right) \end{pmatrix}\mathbf{E}_0, \tag{A.3}$$

where the elements f_{ij} are given by

$$f_{xx} = \frac{\eta_i\left(1-r+\eta_d^2\right)+\frac{\nu_{id}}{\nu_i}\eta_d\left(r-\eta_d\eta_i-1\right)}{\left(\eta_i^2+1\right)\left(\eta_d^2+1\right)+r\left(r-2\eta_d\eta_i-2\right)}, \tag{A.4}$$

$$f_{xy} = \frac{\eta_i^2\left(1+\eta_d^2\right)-r\eta_d\eta_i+\left(\eta_d-\eta_i\right)\frac{\nu_{id}}{\nu_i}\eta_d}{\left(\eta_i^2+1\right)\left(\eta_d^2+1\right)+r\left(r-2\eta_d\eta_i-2\right)}, \tag{A.5}$$

$$f_{zz} = \frac{\left(\eta_i-\eta_d\frac{\nu_{id}}{\nu_i}\right)}{(1-r)} \tag{A.6}$$

with a ratio $r = \frac{\nu_{id}\nu_{di}}{\nu_i\nu_d}$ arising due to ion-dust and dust-ion collisions. If the plasma contains no dust, the elements $f_{xx} = \frac{\eta_i}{\left(\eta_i^2+1\right)}$; $f_{xy} = \frac{\eta_i^2}{\left(\eta_i^2+1\right)}$; $f_{zz} = \eta_i$ corroborate results for a conventional plasma.

Case A: Low gas density : $\eta_e \gg \eta_i > \eta_d > 1$ and $r, \frac{\nu_{id}}{\nu_i} \leq 1$

This limit significantly simplifies the involved expressions for the terms f_{ij}. Retaining the most significant terms they read as

$$f_{xx} \simeq \frac{1}{\eta_i}\left(1+\frac{2r}{\eta_i\eta_d}\right) - \frac{\nu_{id}}{\nu_i}\frac{1}{\eta_i}, \tag{A.7}$$

$$f_{xy} \simeq 1 - \frac{1}{\eta_i^2} - \frac{\nu_{id}\nu_{dn}}{\nu_i\nu_d}\frac{1}{\eta_d\eta_i}, \tag{A.8}$$

$$f_{zz} = \frac{\left(\eta_i - \eta_d\frac{\nu_{id}}{\nu_i}\right)}{(1-r)}. \tag{A.9}$$

Case B: High gas density: $r \ll 1$, $\frac{\nu_{id}}{\nu_i} < 1$ and $\eta_d < \eta_i \leq 10$ while $\eta_e \gg 1$

The elements f_{ij} are now given by

$$f_{xx} \simeq \frac{\eta_i}{(\eta_i^2+1)}\left(1+\frac{\nu_{id}}{\nu_i}\frac{\eta_d\left(\eta_d\eta_i+1\right)}{\eta_i\left(\eta_d^2+1\right)}\right), \tag{A.10}$$

$$f_{xy} \simeq \frac{\eta_i^2}{(\eta_i^2+1)}\left(1-\frac{\nu_{id}}{\nu_i}\frac{\eta_d}{\eta_i\left(\eta_d^2+1\right)}\right), \tag{A.11}$$

$$f_{zz} \simeq \eta_i\left(1-\frac{\nu_{id}}{\nu_i}\frac{\eta_d}{\eta_i}\right). \tag{A.12}$$

580

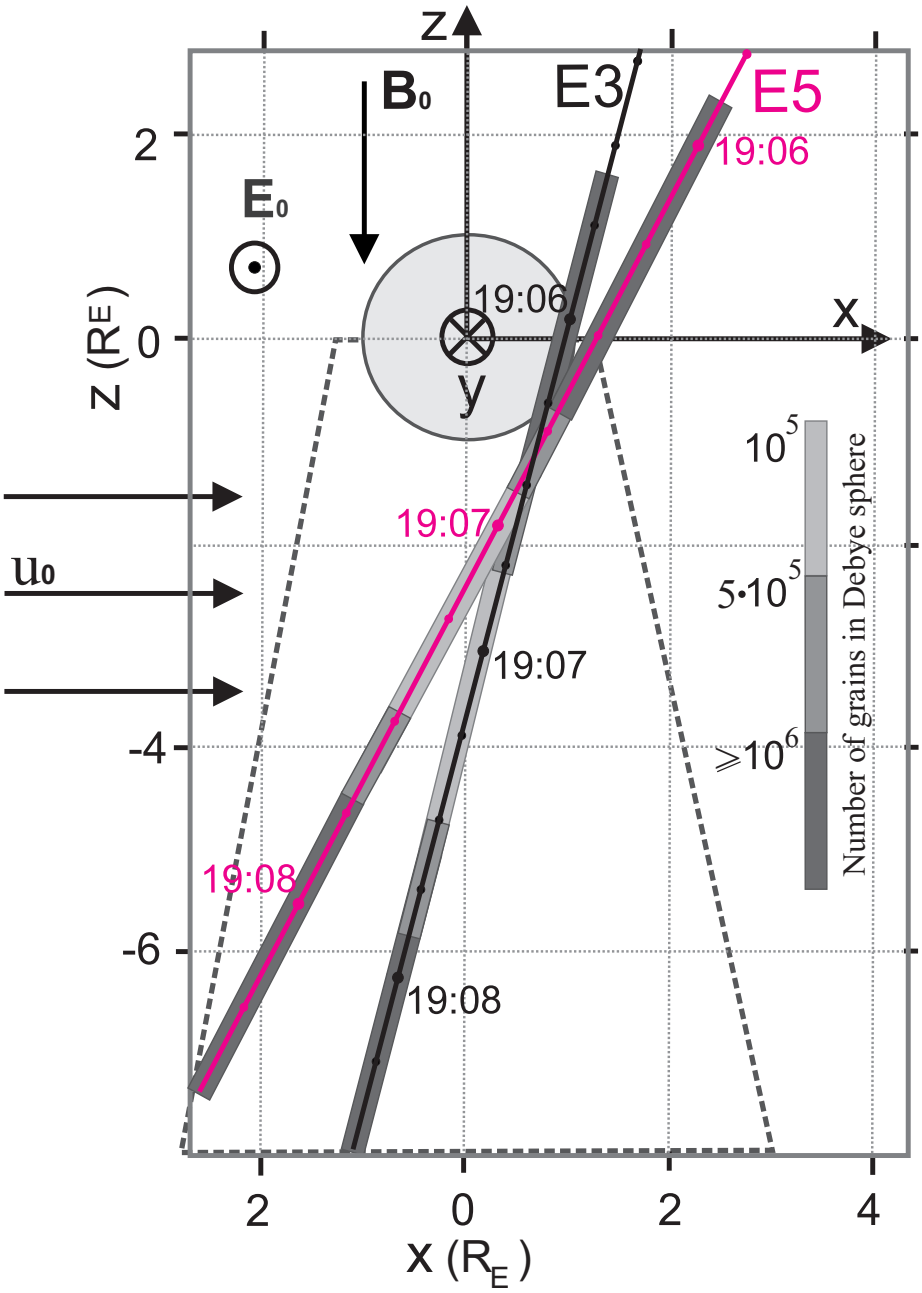

Figure A.1: Schematic of the Enceladus plume and the Enceladus Interaction System (ENIS): $(+x)$ axis is aligned with the direction of ideal co-rotation, the $(+z)$ axis is anti-parallel to the ambient magnetospheric field $\mathbf{B}_0$. The $(+y)$ axis completes the right-handed coordinate system and points towards Saturn, being anti-parallel to the convective electric field in the unperturbed magnetospheric flow upstream of Enceladus $\mathbf{E}_0$. The origin of the ENIS system coincides with the center of the moon. The undisturbed co-rotating ion flow approaches the plume from the left in the diagram (flow vectors labeled u_0). The spacecraft trajectories during the E3 (12 March 2008) and E5 (9 October 2008) encounters are displayed. Variations of the value $N = 4\pi\lambda_{Dd}^3 n_d/3$ (dust plasma parameter) along the E3 and E5 trajectories are shown as gray scale bars quantitatively consistent with the CAPS measurements of the dust density n_d (*Hill et al.*, 2012). The dust Debye length, λ_{Dd} has been calculated assuming the dust temperature $T_d \simeq 200$ K and dust charge $q_d \simeq e$.

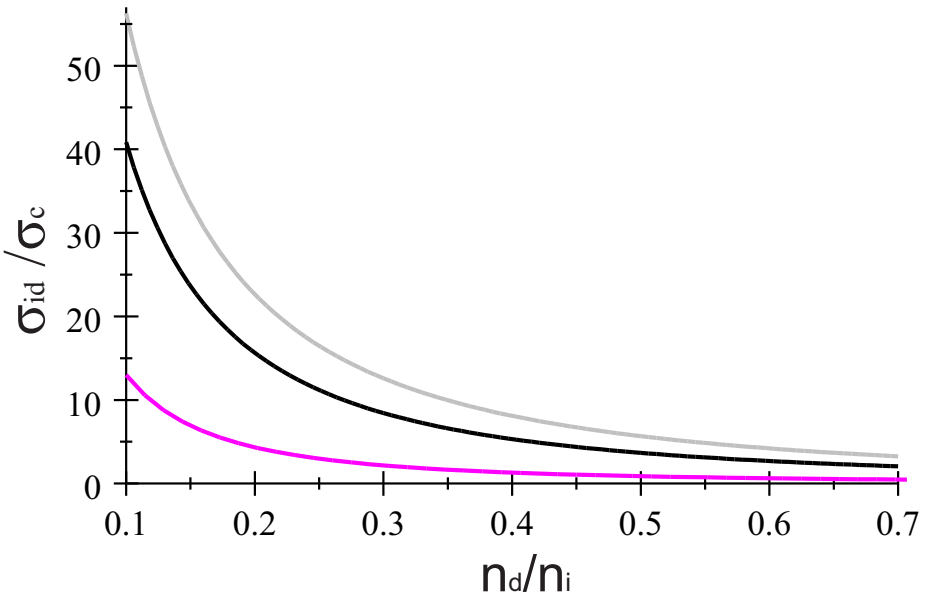

Figure A.2: Cross section ratio σ_{id}/σ_c vs n_d/n_i for nanometer-sized grains: $a = 3$ nm, $T_e = T_i = 1$ eV (gray curve); $a = 2$nm, $T_e = T_i = 2$ eV (black); $a = 3$ nm, $T_e = 2$ eV, $T_i = 3$ eV (magenta); the plasma screening length is taken as $\lambda_D \simeq 30$ cm.

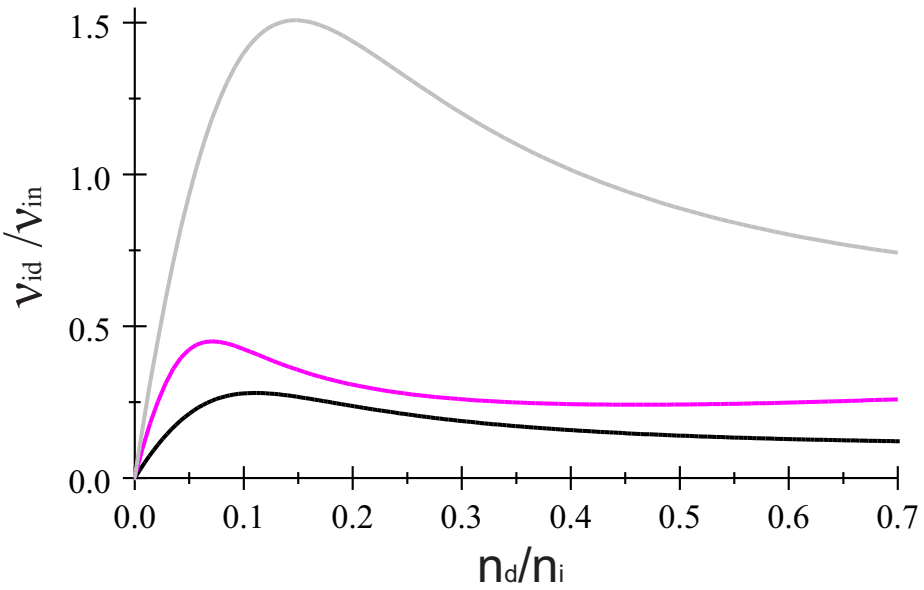

Figure A.3: Momentum transfer frequency ratio ν_{id}/ν_{in} vs n_d/n_i for nanograins at various ionization fractions n_i/n_n. Gray curve: $a = 3$ nm, $T_e = T_i = 1$ eV and magenta curve $a = 3$ nm, $T_e = 2$ eV, $T_i = 3$ eV $n_i/n_n = 10^{-3}$; black curve $a = 2$nm, $T_e = T_i = 2$ eV and $n_i/n_n = 5 \times 10^{-4}$; in all calculations the neutral gas temperature is taken as $T_n \sim 200K$, and the average screening length as $\lambda_D \simeq 30$ cm. **Note, that since $\nu_{id}/\nu_{in} \simeq l_n/l_d$ the presented plots also illustrate variations in the ratio of the ion-neutral collision mean free path to the mean free path in ion-dust collisions, i.e. l_n/l_d vs n_d/n_i.**

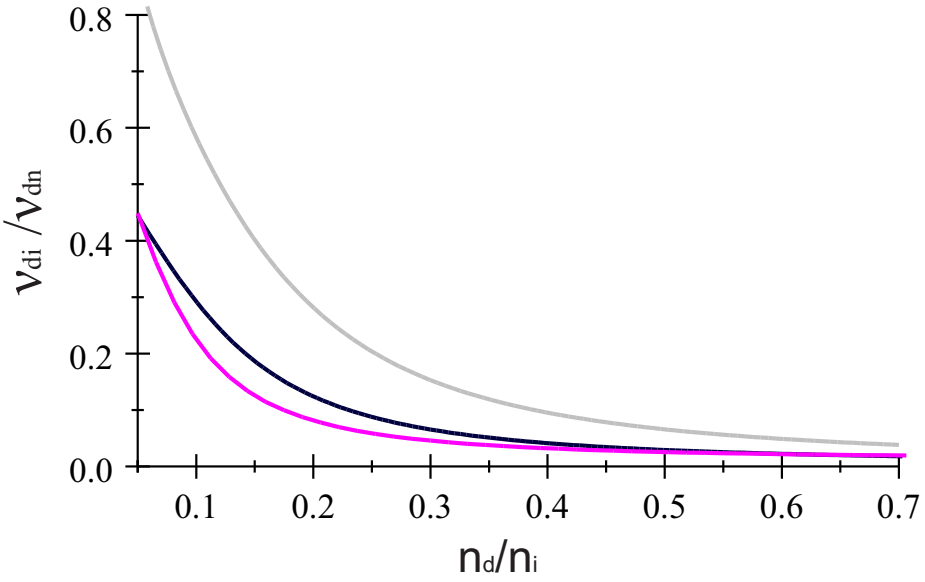

Figure A.4: As in Fig. 3 but for momentum transfer frequency ratio ν_{di}/ν_{dn} vs n_d/n_i.

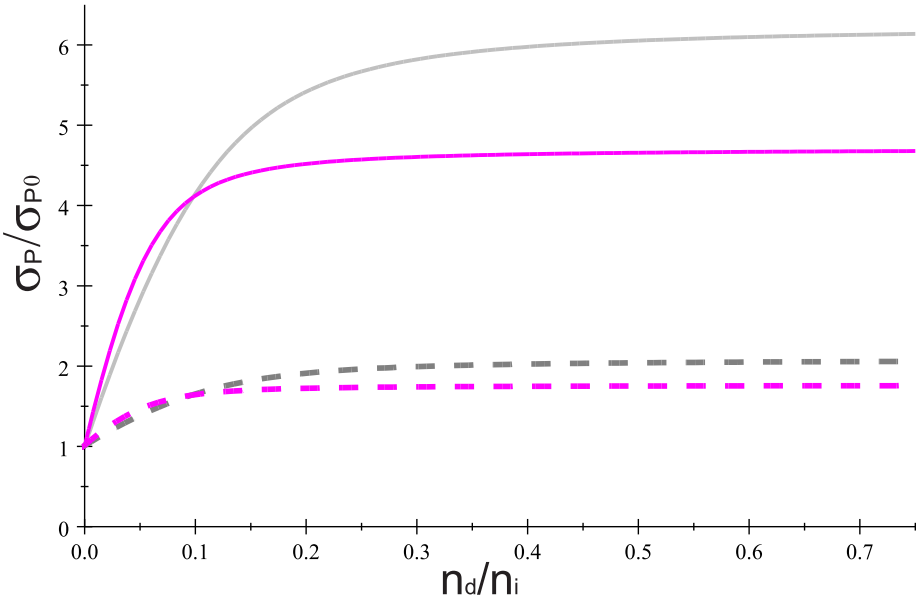

Figure A.5: Normalized Pedersen conductivity σ_P/σ_{P0} vs n_d/n_i. Gray curves: $a = 3$ nm, $T_e = T_i = 1$ eV; magenta curves $a = 3$ nm, $T_e = 2$ eV, $T_i = 3$ eV, $n_i/n_n = 10^{-3}$, other parameters as in Figs. 2-4. Solid curves correspond to the Case A, Eq. (11), dashed ones to Eq. (18) (gas density $n_n = 9 \times 10^8$ cm^{-3}, case B).

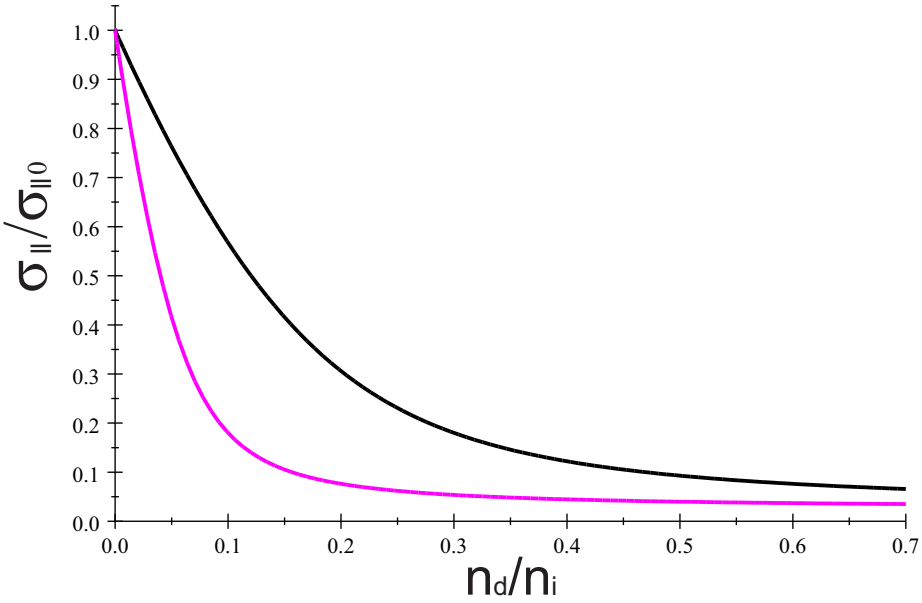

Figure A.6: Normalized parallel conductivity $\sigma_\parallel/\sigma_{\parallel 0}$ vs n_d/n_i. Black curve: $a = 2$ nm, $T_e = T_i = 1$ eV and magenta curve $a = 3$ nm, $T_e = 2$ eV, $T_i = 3$ eV, other parameters as in Figs. 2-4.

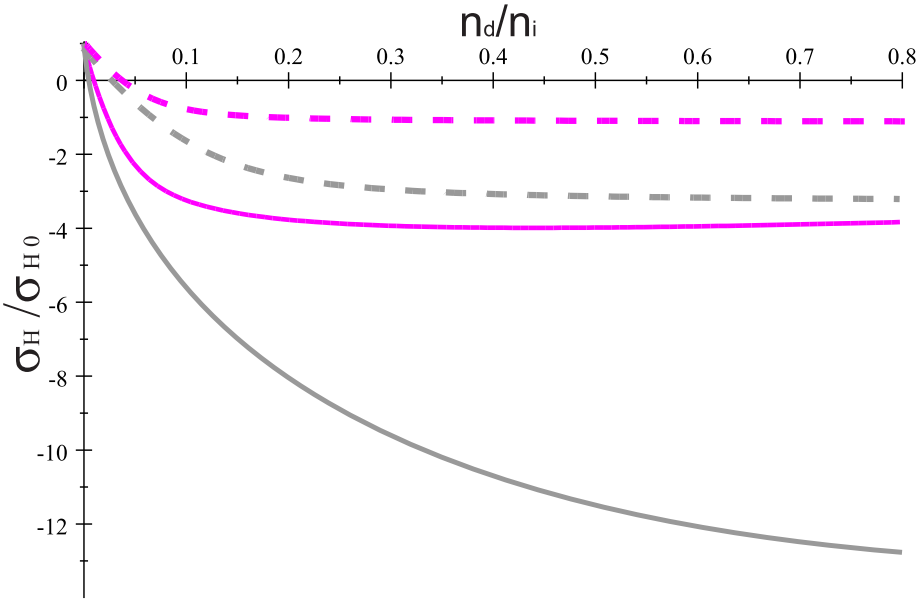

Figure A.7: Normalized Hall conductivity σ_H/σ_{H0} vs n_d/n_i. Gray curves: $a = 3$ nm, $T_e = T_i = 1$ eV; magenta curves: $a = 3$ nm, $T_e = 2$ eV, $T_i = 3$ eV, $n_i/n_n = 10^{-3}$, other parameters as in Figs. 2-4. Solid curves correspond to Eq. (12) (case A), dashed ones to Eq. (19) (gas density $n_n = 9 \times 10^8$ cm^{-3}, case B).

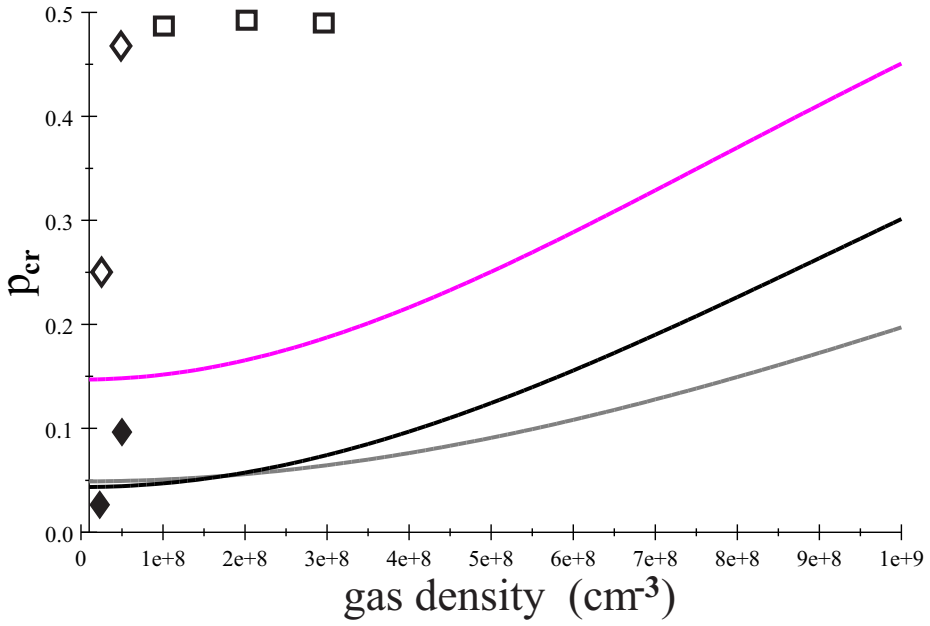

Figure A.8: Dependence of the critical value of the Havnes parameter, p_{cr} defined by Eq. (20), versus neutral gas density, n_n: magenta curve $a = 3$ nm, $T_e = 2, T_i = 3$ eV, black curve: $a = 2$ nm $T_e = T_i = 2$ eV; gray curve: $a = 3$ nm, $T_e = T_i = 1$ eV; other parameters as in Figs. 2-4. Symbols indicate estimates of $p \simeq n_d/n_i$ based on the CAPS measurements of n_d and respective ion densities n_i derived either from interpretations of the Cassini Langmuir probe measurements ((*Morooka et al.*, 2011), solid diamonds) or from hybrid simulations by Kriegel et al. 2014 for E3 (open diamonds) and E5 (open squares) flybys.